mathematics

Article

Numerical Investigation of Radiative Hybrid Nanofluid Flows over a Plumb Cone/Plate

Francis Peter [1], Paulsamy Sambath [1,*] and Seshathiri Dhanasekaran [2,*]

[1] Department of Mathematics, SRM Institute of Science and Technology, Kattankulathur, Chengalpattu 603203, Tamil Nadu, India; fp9469@srmist.edu.in
[2] Department of Computer Science, UiT the Arctic University of Norway, 9037 Tromso, Norway
* Correspondence: sampathp@srmist.edu.in (P.S.); seshathiri.dhanasekaran@uit.no (S.D.)

Abstract: Non-Newtonian fluids play a crucial role in applications involving heat transfer and mass transfer. The inclusion of nanoparticles in these fluids improves the efficiency of heat and mass transfer processes. This study employs a numerical solution approach to examine the flow of non-Newtonian hybrid nanofluids over a plumb cone/plate surface, considering the effects of magnetohydrodynamics (MHD) and thermal radiation. Additionally, we investigate how heat and mass transfer are affected by a fluid containing microorganisms. The governing nonlinear partial differential equations are transformed into nonlinear ordinary differential equations using a similarity transformation to simplify this complex system. We then use the Keller-box finite-difference method to solve these equations. Along with a table presenting the results for skin friction, Nusselt number, Sherwood number, and microbe density number, we present graphical representations of velocity, temperature, concentration, and microorganism diffusion behavior. Our results indicate that the addition of MHD and thermal radiation improves the diffusion of microorganisms, thereby enhancing the rates of heat and mass transfer. Through a comparative analysis with prior research, we demonstrate the reliability of our conclusions.

Keywords: bio-convection; chemical reaction; Eyring–Powell nanofluid; MHD; thermal radiation

MSC: 35Q30; 76W05; 76D10; 76D55; 65N08; 80A20

check for updates

Citation: Peter, F.; Sambath, P.; Dhanasekaran, S. Numerical Investigation of Radiative Hybrid Nanofluid Flows over a Plumb Cone/Plate. *Mathematics* **2023**, *11*, 4331. https://doi.org/10.3390/math11204331

Academic Editor: Andrei D. Polyanin

Received: 11 September 2023
Revised: 5 October 2023
Accepted: 7 October 2023
Published: 18 October 2023

1. Introduction

Various industries commonly employ vertical cones and plate-shaped tools, such as chemical processing, food production, brewing, beverage manufacturing, metalworking, foundries, plastics, and textiles. These tools often require rapid cooling following use to sustain industrial operations. For example, vertical cone/plate mixers play a crucial role in producing high-quality, safe products for people worldwide, including food, medicines, household cleaners, and personal hygiene products. Each vertical cone/plate mixer model is designed with specific industrial objectives in mind. When vertical cone/plate mixers are used, there is a noticeable increase in grinding efficiency, resulting in the mixer's surface warming up on the cone and plate. This heating occurs because the mixture is rapidly and thoroughly mixed, which transports heat along the surface of the cone and plate. This paper describes the heat transfer events and their parametric properties in these situations. The temperature of the heated cone and plate is then convective to its surroundings. In [1,2], the authors discovered that non-Newtonian fluids outperformed conventional fluids in effectively cooling these vertical cone and plate structures. Furthermore, they observed that the introduction of nanofluids containing copper (Cu) and titanium dioxide (TiO_2) enhanced heat transfer efficiency [3,4]. In this context, we focus on the well-known Eyring–Powell, non-Newtonian fluid. Additionally, we investigate how microorganisms influence heat and mass transport processes in the presence of magnetohydrodynamics (MHD) and thermal radiation effects.

Hering and Grosh [5] and Lin [6] used an analytical method to analyze the free convection heat transfer across a cone. Pop and Watanabe [7], Tripathi et al. [8], Hossain et al. [9], Pullepu et al. [10], and Sambath et al. [11] studied free convection flow over cones, focusing on constant heat flux boundary conditions. Bapuji Pullepu et al. [12] integrated uniform surface heat flux into previous works, utilizing the Thomas method for the numerical solutions. Hasan and Mujumdar [13] conducted an analytical analysis of free convection across a vertical cone with heat and mass flux conditions. Sambath et al. [14] explored heat and mass flux conditions and extended the heat and mass transfer models to account for porosity effects. The unsteady nanofluid flow around a cone with uniform heat flux conditions was established by Hajar Hanafi et al. [3] and Ragulkumar et al. [4], and the model was solved using the Crank–Nicolson technique. Their findings demonstrated an increase in heat transfer due to nanofluids. Their study also included non-Newtonian fluid flow and examined the effects of these fluids on free convection in various geometries, a topic also studied by William and Graham [1] and Manisha Patel and Timol [2]. The heat and mass transfer of laminar nanofluid flow over various geometries influenced by MHD and thermal radiation have been studied by some researchers and solved using various methods, including simulations [15], the finite-difference method [16], the finite-element method [17], and the shooting method [18]. The heat and mass transfer of non-Newtonian fluid flow over a porous cone were explored numerically in the works of Kairi and Murthy [19] and Macharla Jayachandra Babu et al. [20]. Numerous studies have examined the non-Newtonian Eyring–Powell fluid flow over a stretching sheet with various important factors to improve heat and mass transfer. The governing equations have been solved using numerical methods such as successive over-relaxation (SOR) [21], Runge–Kutta fourth-order method in combination with the shooting technique [22–25], the finite-element method [26], the Runge–Kutta–Fehlberg numerical scheme [27], the homotopy analysis method [28], and the spectral quasi-linearization method (SQLM) [29]. Currently, the previously discussed numerical methods for fluid flow models yield the best results. Some researchers have also looked at the fluid flow problem's stability and convergence [30,31]. The application of the predictor-corrector method [32] demonstrates excellent accuracy and numerical stability, making it suitable for nonlinear fluid dynamics problems. Another efficient approach for handling the singularity of nonlinear partial differential equations is the Sinc-collocation method [33] together with single exponential (SE) transformation. Finally, several researchers have investigated non-Newtonian nanofluids containing microorganisms. The effects of MHD and thermal radiation models on bio-convective non-Newtonian fluid flow over a stretching surface were studied by Dulal Pal et al. [34], Anas et al. [35], Sreenivasulu et al. [36], and Mahdy [37]. Bio-convective fluid flow over a disc subjected to constant heat, mass, and microorganism boundary conditions was studied by Rahila Naza et al. [38].

The heat and mass transfer of non-Newtonian fluids with various geometrical properties have been studied by many researchers [20,21,27–29]. Additionally, several researchers [3,4] have studied nanofluid flow with various geometrical configurations. In this study, non-Newtonian fluid and nanofluids (Table 1) were combined, and the heat and mass transfer of non-Newtonian nanofluid flow over a vertical cone/plate surface were analyzed. Our literature analysis revealed that bio-convection processes increase heat and mass transfer [34,35]. To improve heat and mass transfer, we also included the profiles of microorganisms in this model. The impacts of MHD, thermal radiation, and chemical processes were also considered to enhance heat and mass transfer. Numerous researchers have solved their models utilizing analytical and semi-analytical techniques, finite-element techniques, Crank–Nicolson techniques, and analytical methods. However, the Eyring–Powell fluid flow model is ineffective with these methods because the solution contains an error if these methods are utilized. To reduce the inaccuracy in this numerical analysis, we used the Keller-box finite-difference scheme for this nonlinear fluid dynamics system.

Table 1. Thermo-physical properties [4] of water and nanoparticles.

Fluid	$\rho\left(\frac{\mathrm{Kg}}{\mathrm{m}^3}\right)$	$Cp\left(\frac{\mathrm{J}}{\mathrm{kgK}}\right)$	$k\left(\frac{\mathrm{W}}{\mathrm{mK}}\right)$	$\bar{\beta}\times 10^{-5}\ (\mathrm{K}^{-1})$
H_2O	997.1	4179	0.613	21
Cu	8933	385	401	1.67
TiO_2	4250	686.2	8.9538	0.9

The remainder of the paper has been divided into the following sections to provide a clear framework for our research. The governing equations, boundary conditions, and mathematical and physical models that constitute the basis of our study problem are examined in detail in Section 2. Section 3 describes our method for solving the governing equations while accounting for the appropriate boundary conditions. Section 4 describes our findings using visually appealing figures to better interpret the problem. Finally, we provide our conclusions on the subject of this research in Section 5. We also emphasize the importance of our findings and suggest potential directions for additional study in this area.

2. Mathematical Model

Consider a steady, two-dimensional, incompressible Eyring–Powell nanofluid flow over a vertical cone/plate in the presence of MHD, thermal radiation, and chemical reactions. The cone has a radius r and half-angle ω. The y-axis is normal to the surface of the cone/plate, and the x-axis varies along the surface of the cone/plate. u and v are the velocity components along the x-axis and y-axis, respectively. Figure 1 illustrates the mathematical model of the system. Consider that the fluid's properties are constant except for the density variation. Following the Boussinesq approximation, the continuity, momentum, energy, and microorganism equations are provided below ([20,21,27–29]).

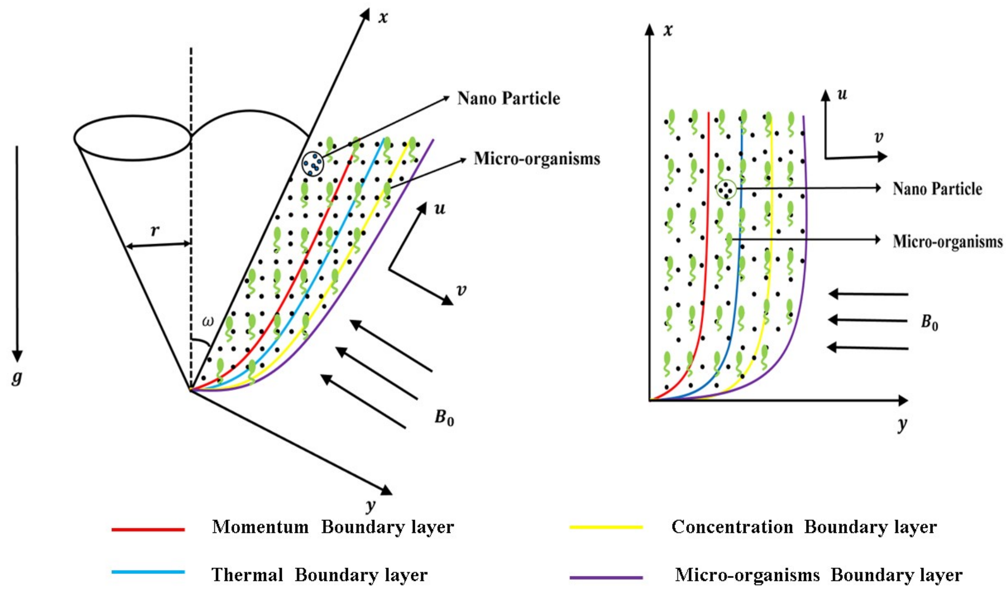

Figure 1. Physical model.

Equation of continuity

$$\frac{\partial(r^a u)}{\partial x}+\frac{\partial(r^a v)}{\partial y}=0 \tag{1}$$

Equation of momentum

$$\left(\rho_{hnf}\right)\left(u\frac{\partial u}{\partial x}+v\frac{\partial u}{\partial y}\right)=\left(-\frac{1}{2\beta d^3}\left(\frac{\partial u}{\partial y}\right)^2\right)\left(\frac{\partial^2 u}{\partial y^2}\right)+\left(\mu_{hnf}+\frac{1}{\beta d}\right)\left(\frac{\partial^2 u}{\partial y^2}\right)$$
$$+\left((\rho\beta_T)_{hnf}(T-T_\infty)+(\rho\beta_C)_{hnf}(C-C_\infty)\right)g cos\omega$$
$$+\left(\gamma(\rho\beta_N)_{hnf}\Delta\rho(N-N_\infty)\right)g cos\omega-\sigma_1(B_0)^2u \tag{2}$$

Equation of energy

$$u\frac{\partial T}{\partial x}+v\frac{\partial T}{\partial y}=\alpha_{hnf}\frac{\partial^2 T}{\partial y^2}-\frac{1}{(\rho c_p)_{hnf}}\left(\frac{\partial q_r}{\partial y}\right) \tag{3}$$

Equation of concentration

$$u\frac{\partial C}{\partial x}+v\frac{\partial C}{\partial y}=D\frac{\partial^2 C}{\partial y^2}-k_c(C-C_\infty) \tag{4}$$

Equation of microorganisms

$$u\frac{\partial N}{\partial x}+v\frac{\partial N}{\partial y}+\frac{bW_c}{(C_w-C_\infty)}\frac{\partial}{\partial y}\left(N\frac{\partial C}{\partial y}\right)=D_n\frac{\partial^2 N}{\partial y^2} \tag{5}$$

The boundary conditions are

$$\begin{aligned} u=0, v=0, T=T_w, C=C_w, N=N_w \quad at \quad y=0 \\ u\to 0, T\to T_\infty, C\to C_\infty, N\to N_\infty \quad as \quad y\to\infty \end{aligned} \tag{6}$$

The radiative heat flux q_r is employed according to the Rosseland approximation [21] so that

$$q_r=-\frac{4\sigma^*}{3k^*}\frac{\partial T^4}{\partial y}$$

where σ^* is the Stefan–Boltzmann constant and k^* is the mean absorption coefficient. Following Ragulkumar et al. [16], we assume that the temperature difference within the flow is small, so T^4 can be expressed as a linear function of the temperature. Expanding T^4 into a Taylor series about T^∞ and neglecting higher-order terms, we have $T^4 \simeq 4T_\infty^3 T - 3T_\infty^4$. When $a=0$, it means that it is a vertical plate, and when $a\neq 0$, it means that it is a vertical cone. By using the following similarity transformations, the governing nonlinear differential Equations (1)–(6) can be transformed into a set of nonlinear ordinary differential equations: $\Psi=\nu_f r(Gr)^{1/4}.f(\xi)$, $\xi=\frac{y}{x}(Gr)^{1/4}$, $u=\frac{\nu_f}{x}(Gr)^{1/4}.f'(\xi)$, $v=\frac{\nu_f}{4x}(Gr)^{1/2}[\xi.f'(\Psi)-7f(\xi)]$, $Gr=\frac{g\beta_T(T_w-T_\infty).x^3}{\nu_f^2}$, $\theta(\xi)=\frac{T-T_\infty}{T_w-T_\infty}$, $\varphi_(\xi)=\frac{C-C_\infty}{C_w-C_\infty}$, $\chi(\xi)=\frac{N-N_\infty}{N_w-N_\infty}$, $r=xsin\omega$.

By using the similarity transformations, the dimensionless forms of the momentum, energy, concentration, and diffusion of microorganisms are as follows:

$$\left(\frac{1}{A_2}\right)\left(A_1+K-KN_1(f'')^2\right)f'''-\left(\left(\frac{1}{2}\right)f'^2-\left(\frac{7}{4}\right)ff''\right)$$
$$+A_3(\theta+N_r\varphi+R_b\,\chi)cos\omega-\frac{M}{A_2}f'=0 \tag{7}$$

$$\left(\frac{1}{\Pr}\right)A_4\left(\frac{k_{hnf}}{k_f}+\left(\frac{4}{3}\right)R_d\right)\theta''+\left(\frac{7}{4}\right)f\theta'=0 \tag{8}$$

$$\left(\frac{1}{S_c}\right)\varphi'' + \left(\frac{7}{4}\right)f\varphi' - K_r\varphi = 0 \tag{9}$$

$$\chi'' + \left(\frac{7}{4}\right)L_b f\chi' - P_e\left(\chi'.\varphi' + (\chi+\sigma)\varphi''\right) = 0 \tag{10}$$

The corresponding boundary conditions are as follows:

$$\begin{aligned} f(0) = 0,\ f'(0) = 0,\ \theta(0) = 1,\ \varphi_(0) = 1,\ \chi(0) = 1 \quad at \quad \xi = 0 \\ f'(\xi) \to 0, \quad \theta(\xi) \to 0, \quad \varphi(\xi) \to 0, \quad \chi(\xi) \to 0 \quad as \quad \xi \to \infty \end{aligned} \tag{11}$$

where $K = \left(\frac{1}{\mu_f \mathrm{d}\beta}\right)$, $N_1 = \frac{\nu_f^2(\mathrm{Gr})^{\frac{3}{2}}}{2d^2x^4}$, $N_r = \frac{\beta_C(C_w - C_\infty)}{\beta_T(T_w - T_\infty)}$, $R_b = \frac{\beta_N(N_w - N_\infty)\Delta\rho\gamma}{\beta_T(T_w - T_\infty)}$, $R_d = \frac{4\sigma^*.T^3}{k^*.k_f}$, $K_r = \frac{k_c x^2}{\nu_f(Gr)^{1/2}}$, $S_c = \frac{\nu_f}{D}$, $Pr = \frac{\nu_f}{\alpha_f}$, $L_b = \frac{\nu_f}{D_n}$, $P_e = \frac{bW_c}{D_n}$, $\sigma = \frac{N_\infty}{N_w - N_\infty}$, $M = \frac{\sigma_1.B_0^2(Gr)^{-1/2}x^2}{\mu_f}$, $A_1 = \left[\frac{1}{(1-\phi_1)^{2.5}(1-\phi_2)^{2.5}}\right]$, $A_4 = \phi_2\frac{(\rho c_p)_{s_2}}{(\rho c_p)_f} + (1-\phi_2)[(1-\phi_1) + \phi_1\frac{(\rho c_p)_{s_1}}{(\rho c_p)_f}\Big]$, $A_2 = \phi_2\frac{\rho_{s_2}}{\rho_f} + \left[(1-\phi_2)\left((1-\phi_1) + \phi_1\frac{\rho_{s_1}}{\rho_f}\right)\right]$, $A_3 = \frac{\phi_2\frac{\beta\rho_{s_2}}{\beta\rho_f} + \left[(1-\phi_2)\left((1-\phi_1)+\phi_1\frac{\beta\rho_{s_1}}{\beta\rho_f}\right)\right]}{\phi_2\frac{\rho_{s_2}}{\rho_f} + \left[(1-\phi_2)\left((1-\phi_1)+\phi_1\frac{\rho_{s_1}}{\rho_f}\right)\right]}$.

In dimensionless forms, the local skin friction coefficient C_f, the local Nusselt number Nu, the local Sherwood number Sh, and the density of the microorganisms Nn are as follows:

$$\begin{aligned} (Gr)^{1/4}C_f = (A_1 + K)f''(0) - \frac{KN_1}{3}(f''(0))^3), \quad (Gr)^{-1/4}Sh = -\varphi'(0), \\ (Gr)^{-1/4}Nu = -\left(\frac{k_{hnf}}{k_f} + \frac{4}{3}R_d\right)\theta'(0), \quad (Gr)^{-1/4}Nn = -\chi'(0). \end{aligned}$$

3. Numerical Investigation

The Keller-box technique is an efficient finite-difference method used for solving parabolic problems, especially those involving systems of nonlinear coupled ordinary differential equations (ODEs). We can solve the higher-order nonlinear problem through following the steps:

- Initially, the nonlinear coupled ODE system is transformed into a system of first-order coupled ODEs.
- Then, an appropriate finite-difference scheme is applied to discretize these equations.
- To linearize the equations, Newton's method is employed during the discretization process.
- Finally, the resulting linear equation system is solved using the block elimination method.

Choosing suitable initial guesses is crucial for achieving convergence and minimizing errors. In this context, the following initial guesses are utilized:

$$f_0'(\xi) = 1 - e^{-\xi}, \quad \theta_0(\xi) = e^{-\xi}, \quad \varphi_0(\xi) = e^{-\xi}, \quad \chi_0(\xi) = e^{-\xi}.$$

In this method, an error tolerance of 10^{-6} is maintained for accurate solutions, and a step size of $h_j = 0.005$ is utilized that yields satisfactory convergence. The results for the numerous parameter changes shown in Tables 2 and 3 indicate excellent agreement, confirming the method's validity. These results provide strong evidence for the efficiency of our finite-difference Keller-box methodology.

Table 2. Comparison of existing results while keeping $\phi_1 = 0$, $\phi_2 = 0$, $K = 0$, $N_1 = 0$, $M = 0$, $R_d = 0$, $K_r = 0$, $R_b = 0$, $L_b = 0$, $P_e = 0$, $P_r = 0$.

		Hasan et al. [13]			Present		
S_c	N_r	C_f	$-\theta(0)$	$-\varphi(0)$	C_f	$-\theta(0)$	$-\varphi(0)$
0.22	0.5	1.37711	0.80133	0.50138	1.38831	0.82104	0.50148
0.22	1	1.76577	0.88024	0.4839	1.76891	0.89099	0.49861
0.22	2	2.40849	0.98391	0.47367	2.44961	0.99801	0.49763

Table 3. Comparison of existing results while keeping $\phi_1 = 0$, $\phi_2 = 0$, $K = 0$, $N_1 = 0$, $M = 0$, $R_d = 0$, $S_c = 0$, $K_r = 0$, $R_b = 0$, $L_b = 0$, $N_r = 0$, $P_e = 0$.

	Lin [6]		Present	
P_r	C_f	$-\theta(0)$	C_f	$-\theta(0)$
0.72	0.889301	1.52278	0.937134	1.570613
1	0.784465	1.391746	0.832299	1.439581
2	0.652528	1.162097	0.700363	1.209932
4	0.463073	0.980958	0.510909	1.028794
6	0.396883	0.891957	0.444721	0.939794
8	0.355639	0.834979	0.403477	0.882817
10	0.326555	0.793885	0.374394	0.841724
100	0.133715	0.483722	0.181555	0.531562

4. Results and Discussion

The heat and mass transfer of bio-convective fluid flow are depicted graphically in this model. All of the parameter values in this model were set as follows: $\phi_1 = 0.01$, $\phi_2 = 0.02$, $K = 0.3$, $N_1 = 2$, $R_d = 0.5$, $K_r = 0.3$, $S_c = 1$, $N_r = 0.5$, $L_b = 0.7$, $P_e = 0.4$, $\sigma = 0.3$, $R_b = 0.3$, $P_r = 6.2$, and $M = 1$. Unless stated otherwise, all the values were fixed [18]. Across all the depicted figures, the three initial curves represent the vertical plate ($\omega = 0$), whereas the three subsequent curves represent the vertical cone ($\omega \neq 0$).

4.1. Velocity Profile

Figure 2 shows a significant inverse correlation between the velocity profile and the Eyring–Powell fluid parameter (K). Compared to the cone, this phenomenon is most evident in the context of the vertical plate, primarily due to the frictional drag force. It is important to note that the cone has a more significant effect on the velocity of the fluid flow compared to the vertical plate. The velocity profile is simplified in Figure 3, where the magnetohydrodynamics (MHD) parameter (M) varies for both the cone and plate geometries. The Lorentz force, which acts perpendicular to the direction of fluid flow, is responsible for this change in the velocity profile. As a result, it causes the momentum boundary layer thickness for the cone and plate to increase. Finally, as the bio-convection Rayleigh number (R_b) and the buoyancy ratio parameter (N_r) increase, an enhanced velocity profile can be observed on the cone and plate surfaces in Figures 4 and 5. An increase in the latter parameters improves momentum transfer within the fluid, resulting in a higher velocity profile. The buoyancy ratio parameter represents the ratio of buoyancy to viscous forces in the fluid flow.

In Table 4, we can see that increasing the volume fraction (both ϕ_1 and ϕ_2) leads to a decrease in local skin friction on both the cone and plate surfaces. Similarly, increasing the Eyring–Powell fluid parameter (K) and MHD parameter (M) yields higher skin friction numbers on both the cone and plate. Furthermore, increasing the buoyancy ratio parameter (N_r) and bio-convection Rayleigh number (R_b) leads to an increase in local skin friction.

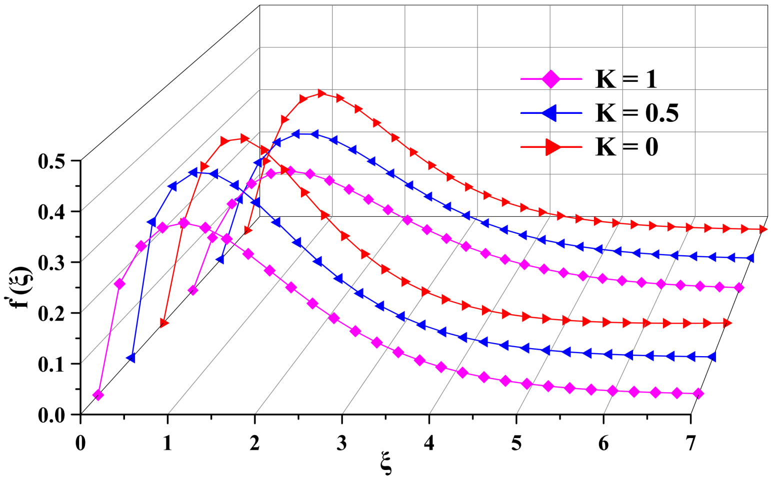

Figure 2. Effect of K on velocity.

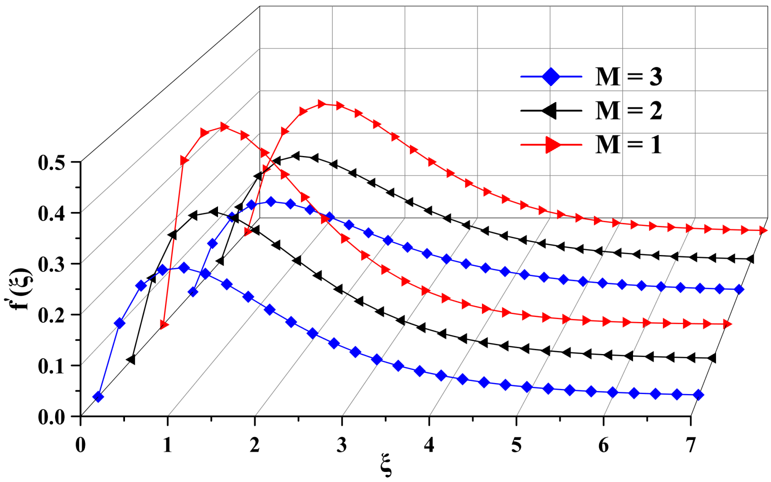

Figure 3. Effect of M on velocity.

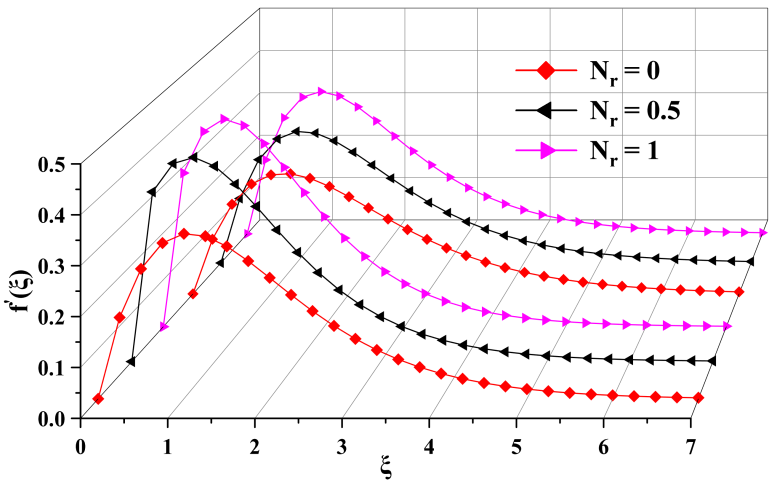

Figure 4. Effect of N_r on momentum.

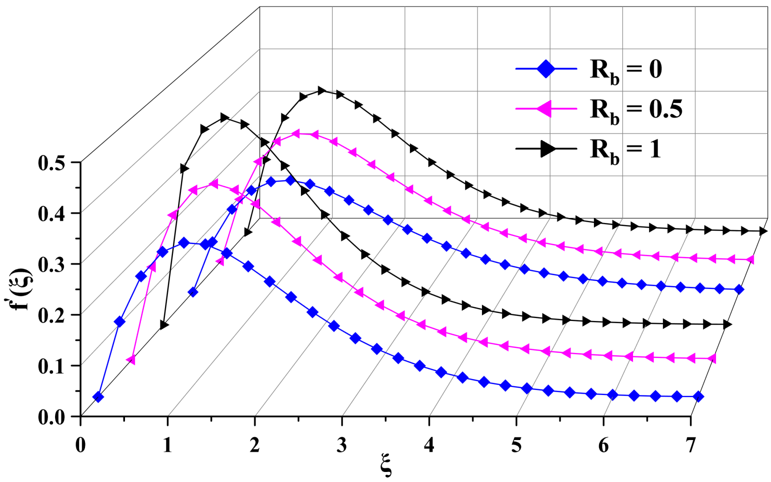

Figure 5. Effect of R_b on velocity.

Table 4. Local skin friction and local Nusselt number.

								C_f		$-\theta'(0)$	
ϕ_1	ϕ_2	K	M	N_r	R_b	R_d	P_r	**Plate**	**Cone**	**Plate**	**Cone**
0.01	0.02	0.3	1	0.5	0.6	0.5	1	1.131153	0.88863	0.690365	0.618286
0.02								1.1364	0.889511	0.682759	0.611744
0.03								1.141152	0.890263	0.675301	0.605313
	0.01							1.123452	0.886061	0.689833	0.617696
	0.02							1.131153	0.88863	0.690365	0.618286
	0.03							1.138383	0.891065	0.690956	0.618927
		0						1.150313	0.859845	0.710972	0.637339
		0.4						1.139797	0.903332	0.684057	0.612581
		0.8						1.209694	0.970576	0.661418	0.592399
			1					1.131153	0.88863	0.690365	0.618286
			2					1.02103	0.780998	0.623575	0.551223
			3					0.935983	0.704455	0.572327	0.501712
				0.5				1.131153	0.88863	0.690365	0.618286
				1				1.265612	1.021415	0.726624	0.650527
				1.5				1.357137	1.137834	0.759688	0.679905
					0.5			1.098349	0.858541	0.681443	0.610087
					1			1.245755	1.001416	0.723507	0.648682
					1.5			1.347483	1.12517	0.760398	0.682358
						0		1.098573	0.860133	0.522744	0.468647
						0.5		1.131153	0.88863	0.690365	0.618286
						1		1.151615	0.906624	0.828881	0.742202
							0.5	1.172796	0.92529	0.508209	0.455492
							1	1.131153	0.88863	0.690365	0.618286
							1.5	1.104223	0.865059	0.822411	0.737154

4.2. Temperature Profile

Figures 6 and 7 show that the temperature of the system increases as the amount of hybrid nanofluid increases, as indicated by the volume fractions ϕ_1 and ϕ_2. This means that heat transfer enhancement occurs at more significant volumes of this fluid mixture. In addition, the cone shape works better in heat transfer compared to the flat plate because the cone's surface has better fluid flow characteristics. The Eyring–Powell fluid parameter (K), which is an important parameter, is highlighted in Figure 8. Improved heat transport is associated with an increase in this parameter. Additionally, compared to a flat plate, the cone shape reveals a thinner layer of warm fluid on its surface, making it more effective at transferring heat. Figure 9 illustrates how increasing the magnetohydrodynamics (MHD) parameter (M) improves heat transfer. This improvement is due to the interaction of the magnetic field with tiny charged particles within the electrically conducting fluid. The electric current produced by these particles leads to the formation of an electric field, which affects the velocity of the liquid and enhances heat transfer. Figure 10 graphically depicts the effect of thermal radiation (R_d) on temperature. Furthermore, an increase in this parameter causes more significant heat transfer because as a fluid's temperature increases over that of its surroundings, it generates electromagnetic waves as heat radiation. According to the Stefan–Boltzmann law, the rate of radiation emission is inversely proportional to the fluid's temperature. Other substances in the fluid or its surroundings can absorb these waves, thereby increasing their temperature and enhancing heat transfer. Finally, Figure 11 shows various Prandtl number (P_r) values, which provide information about the behavior of heat and the momentum in the fluid flow. Heat transfer is affected by the thickness of the heated fluid layer near the surface, which increases as the Prandtl number rises.

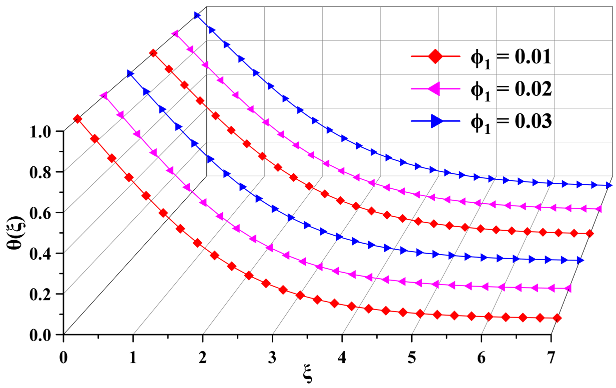

Figure 6. Effect of ϕ_1 on temperature.

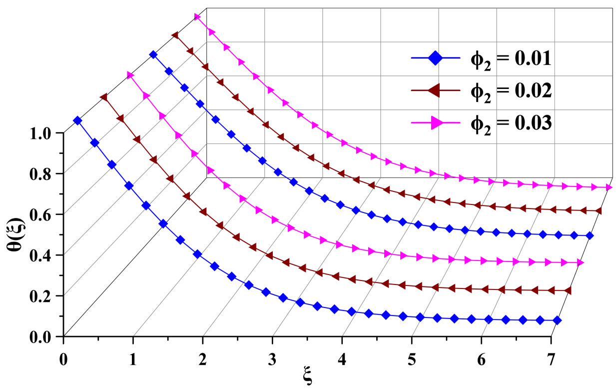

Figure 7. Effect of ϕ_2 on temperature.

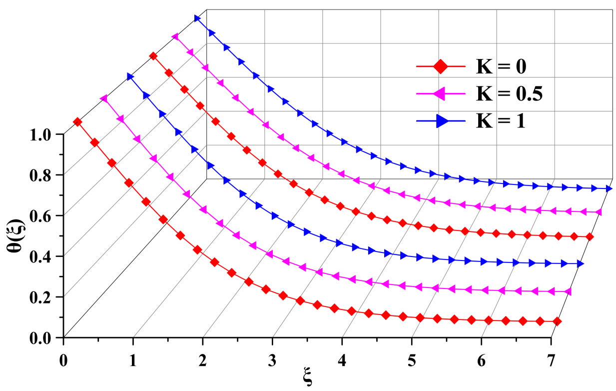

Figure 8. Effect of K on temperature.

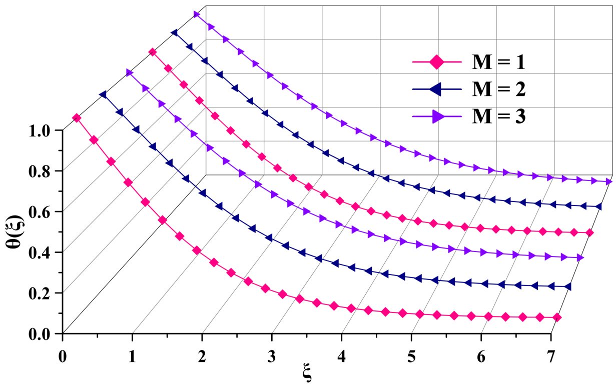

Figure 9. Effect of M on temperature.

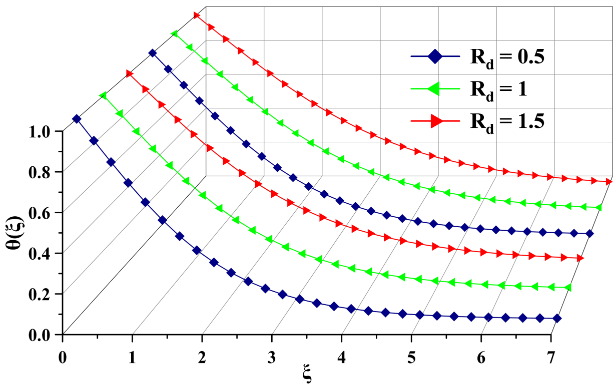

Figure 10. Effect of R_d on temperature.

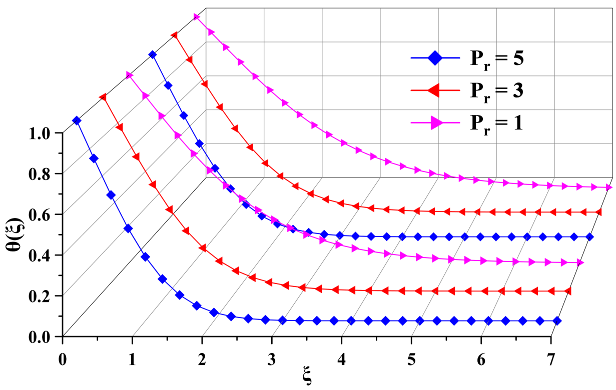

Figure 11. Effect of P_r on temperature.

The cone's superior heat transfer capacity over the flat plate is a consequence of how fluids behave. The fluid slows down over a flat plate, forming a thick boundary layer restricting heat transfer. A curved surface, such as a cone, forces the fluid to accelerate and follow its curvature, resulting in a thinner boundary layer and more significant heat transfer. Further improving heat transfer rates is the cone's higher area of coverage. Referring to Table 4, it is evident that increasing the volume fractions (ϕ_1 and ϕ_2) results in an improved heat transfer rate on both the cone and plate surfaces. The plate exhibits a higher Nusselt number when comparing the cone and plate, indicating better heat transfer performance. Furthermore, increasing the Eyring–Powell fluid parameter (K) and MHD parameter (M) decreases the local Nusselt number for both the cone and plate surfaces. Additionally, an increase in the Prandtl number (P_r) and thermal radiation (R_d) are associated with a higher local Nusselt number.

4.3. Concentration Profile

Figures 12 and 13 show that a fluid substance expands more quickly when the quantity of nanoparticles (represented by volume fractions ϕ_1 and ϕ_2) increases. This occurs due to the resistance these particles introduce, impeding the motion of molecules and influencing the material's dispersion within the fluid. Even a slight increase in the Eyring–Powell fluid parameter (K), as shown in Figure 14, leads to a more efficient concentration process. This is because this parameter elevates the fluid's internal stress, thereby improving mixing and diffusion. Figure 15 shows the results of applying the magnetohydrodynamics (MHD) effect, which causes the concentration boundary layer thickness to decrease and the mass transfer to increase. The MHD increases fluid mixing, which increases the effectiveness of concentration diffusion. In Figure 16, it can be seen that increasing a parameter associated with chemical reactions (K_r) in fluid flow causes more concentration diffusion. In Figure 17, we can see the Schmidt number (S_c) and its explicit representation of the ratio between mass diffusivity and momentum diffusivity in the fluid flow. The concentration boundary layer thickness reaches its maximum value as the Schmidt number (S_c) increases.

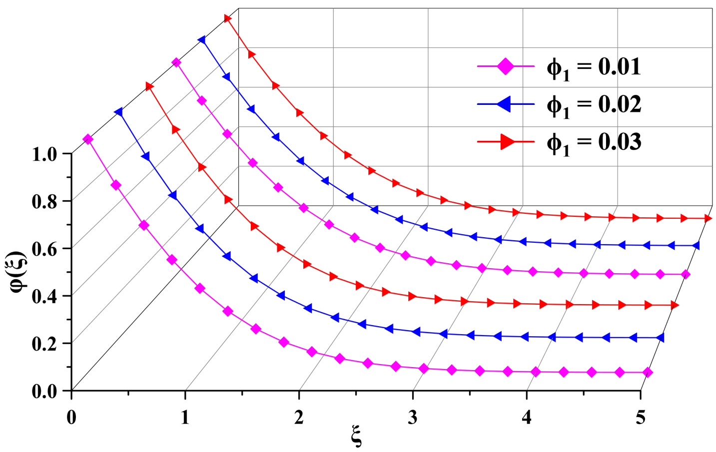

Figure 12. Effect of ϕ_1 on concentration.

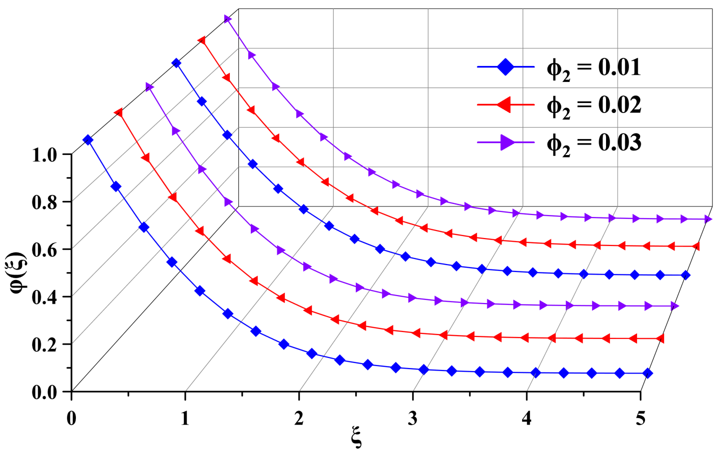

Figure 13. Effect of ϕ_2 on concentration.

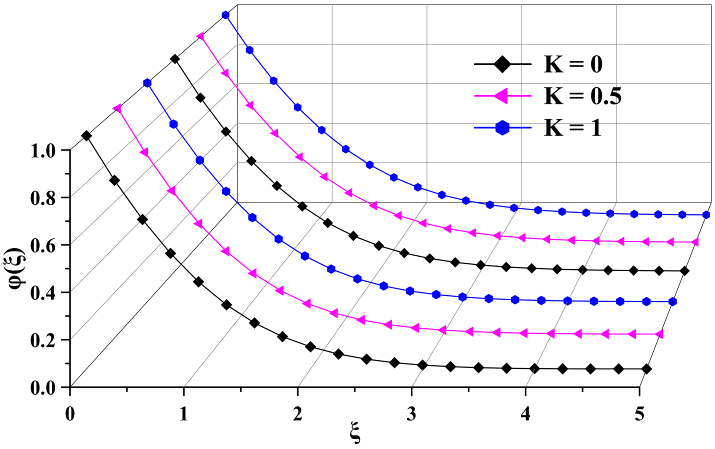

Figure 14. Effect of K on concentration.

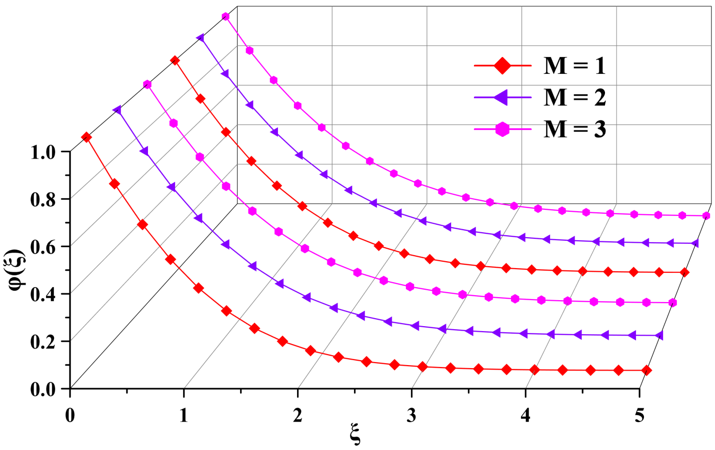

Figure 15. Effect of M on concentration.

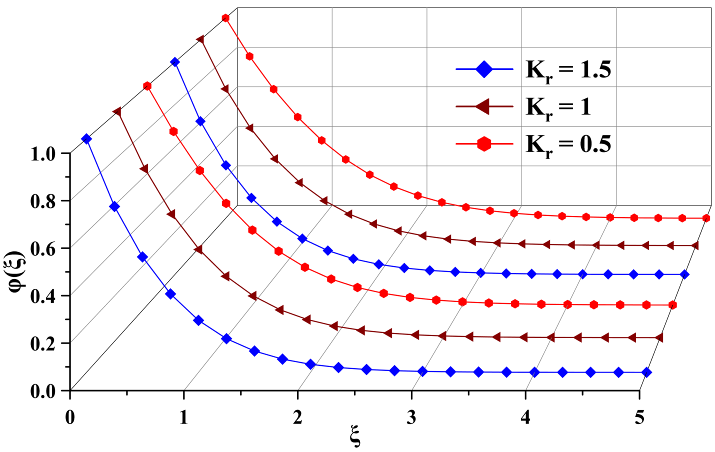

Figure 16. Effect of K_r on concentration.

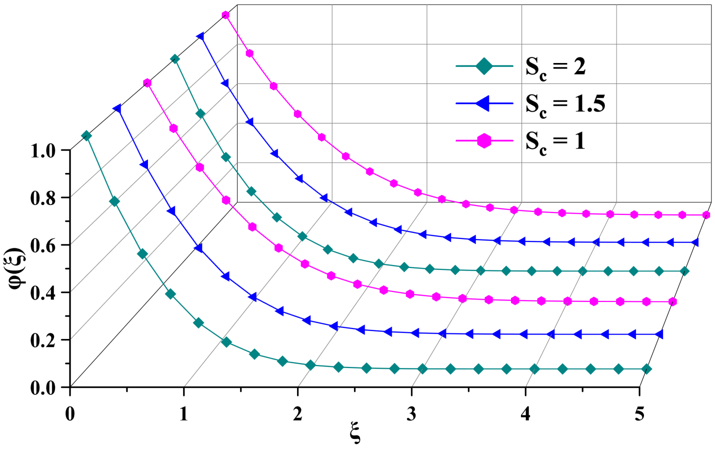

Figure 17. Effect of S_c on concentration.

The flat plate remains constant while the cone varies in size as you move along. The concentration diffusion compared to a flat plate and the rate at which the fluid flows over the cone are both impacted by this size difference. Because the fluid spreads as far to cover the same area as the flat plate, a higher concentration diffusion is close to the cone's surface. It accelerates the movement of the fluid and alters the concentration of the substance relative to the surface of the cone. In Table 5, it is evident that increasing the volume fractions (ϕ_1 and ϕ_2) leads to a decrease in the local Sherwood number on both the cone and plate surfaces. The plate exhibits a higher Sherwood number when comparing the cone and plate, indicating more efficient mass transfer. Furthermore, an increase in the Eyring–Powell fluid parameter (K) and magnetohydrodynamics (MHD) parameter (M) results in a decrease in the local Sherwood number for both the cone and plate surfaces. However, an increase in the chemical reaction parameter (K_r) and Schmidt number (S_c) leads to an increase in the local Sherwood number. These parameters have a positive impact on mass transfer, enhancing the efficiency of the process.

Table 5. Local Sherwood number and local density of microorganisms.

								$-\varphi'(0)$		$-\chi'(0)$	
ϕ_1	ϕ_2	K	M	K_r	S_c	L_b	P_e	Plate	Cone	Plate	Cone
0.01	0.02	0.3	1	0.5	1	0.7	0.5	0.738834	0.702393	0.675461	0.622874
0.02								0.735543	0.699755	0.670701	0.618936
0.03								0.732311	0.697156	0.666022	0.615053
	0.01							0.741197	0.704326	0.678756	0.625622
	0.02							0.738834	0.702393	0.675461	0.622874
	0.03							0.73648	0.700463	0.672178	0.620129
		0						0.752952	0.714813	0.694793	0.640129
		0.4						0.734631	0.69879	0.669685	0.617839
		0.8						0.719995	0.686462	0.649478	0.600492
			1					0.738834	0.702393	0.675461	0.622874
			2					0.709718	0.675568	0.632289	0.581244
			3					0.688489	0.656867	0.599717	0.550899
				0				0.53856	0.484494	0.556124	0.497874
				0.5				0.852076	0.822183	0.752014	0.701389
				1				1.092013	1.071379	0.941386	0.892903
					0.5			0.533732	0.506574	0.5859	0.536361
					1			0.738834	0.702393	0.675461	0.622874
					1.5			0.888363	0.846174	0.760501	0.703905

Table 5. *Cont.*

								$-\varphi'(0)$		$-\chi'(0)$	
ϕ_1	ϕ_2	K	M	K_r	S_c	L_b	P_e	**Plate**	**Cone**	**Plate**	**Cone**
						0.5		0.742074	0.705006	0.62595	0.578825
						1		0.735416	0.699588	0.737577	0.678324
						1.5		0.731674	0.696475	0.821288	0.753207
							0.3	0.741308	0.704506	0.58893	0.538636
							0.6	0.737661	0.701392	0.717649	0.663927
							0.9	0.734372	0.69859	0.840359	0.783281

4.4. Microorganism Profile

In Figure 18, it can be seen that an increase in the Eyring–Powell fluid parameter (K) accelerates the diffusion of microorganisms. This implies that the unique behavior of the fluid, which deviates from the behavior of typical fluids (non-Newtonian behavior), influences the movement and dispersion of microorganisms. Figure 19 demonstrates that applying magnetohydrodynamics (MHD) to a fluid containing microorganisms enhances their diffusion rate and reduces the thickness of the microorganisms' diffusion boundary layer. MHD occurs due to the interaction between a magnetic field and the moving fluid, generating electric currents that facilitate the mixing and dispersion of microorganisms. In Figure 20, it can be seen that an increase in the parameter associated with chemical reactions (K_0) leads to a thinner microorganism boundary layer, primarily due to the increased occurrence of chemical reactions. Figure 21 highlights the impact of thermal radiation on the surrounding fluid's temperature and density near microorganisms. This temperature-induced density variation can induce fluid motion, as warm, lighter fluid rises while more relaxed, denser fluid sinks. These flows affect the distribution of substances around microorganisms. In Figure 22, it can be seen that when microorganisms diffuse within the fluid, an increase in the bio-convection Peclet number (P_e) results in more effective fluid mixing. Lastly, Figure 23 shows that an increase in the Lewis number (L_b) affects bio-convection stability and pattern formation. With a higher Lewis number (L_b), thermal diffusion becomes more dominant than mass diffusion. This alteration in the balance of diffusion mechanisms affects the buoyancy forces that drive bio-convection, reducing stability in the bio-convection patterns.

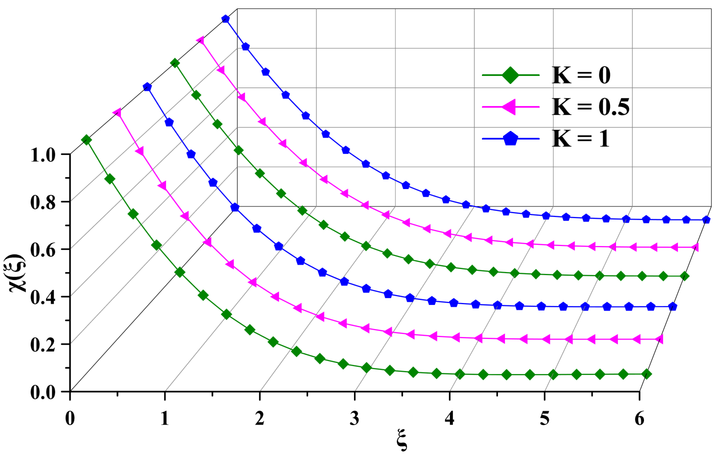

Figure 18. Effect of K on microorganisms.

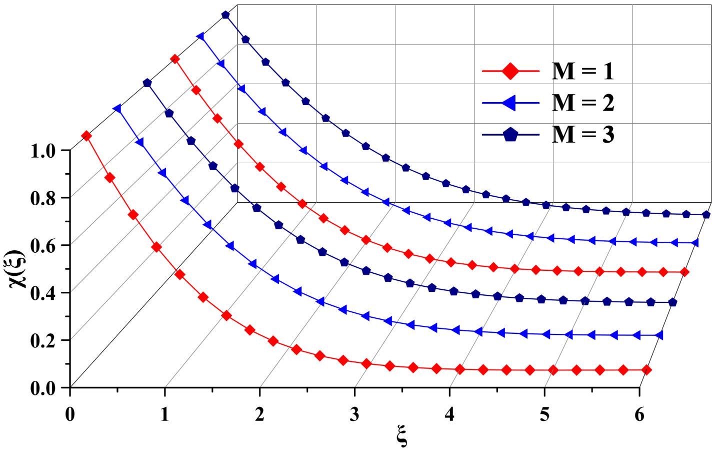

Figure 19. Effect of M on microorganisms.

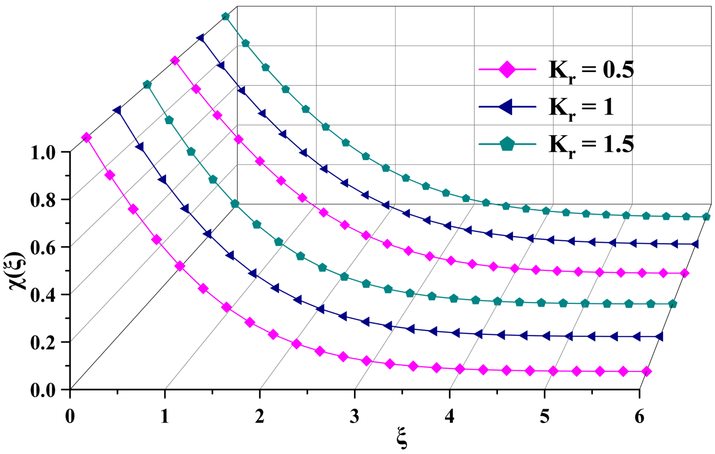

Figure 20. Effect of K_r on microorganisms.

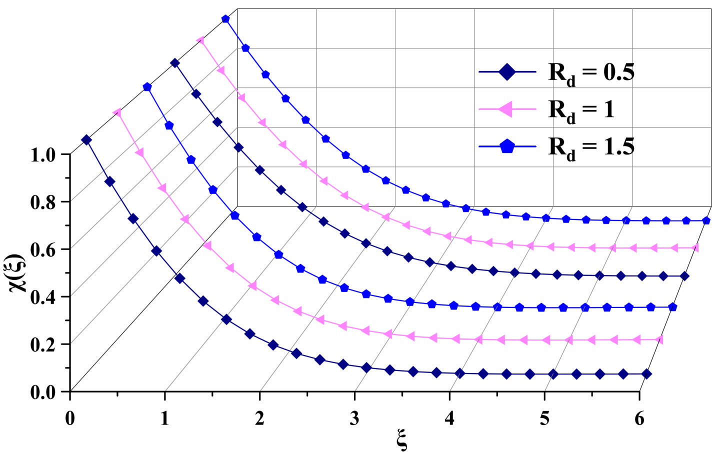

Figure 21. Effect of R_d on microorganisms.

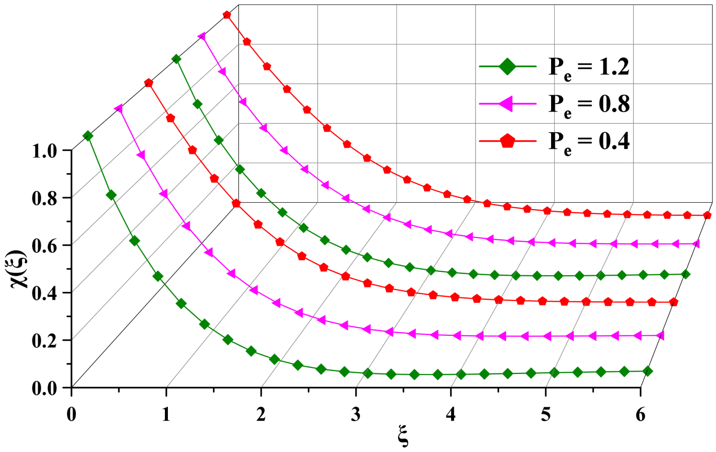

Figure 22. Effect of P_e on microorganisms.

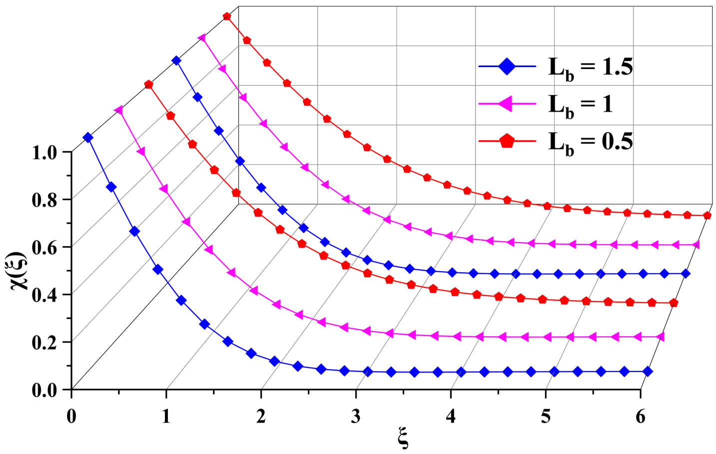

Figure 23. Effect of L_b on microorganisms.

Overall, Figures 18–23 indicate that the diffusion rate of microorganisms is typically higher on a cone surface than on a vertical plate. The larger surface area of the cone is responsible for providing more opportunities for microorganisms to interact with the fluid and promoting enhanced diffusion. In Table 5, we can see that increasing the Eyring–Powell fluid parameter (K) and magnetohydrodynamics parameter (M) for both the cone and plate surfaces results in a decrease in the local microorganisms' density number. Conversely, increases in the chemical reaction parameter (K_r), bio-convection Peclet number (P_e), and bio-convection Lewis number (L_b) lead to an increase in the local microorganisms' density number.

5. Conclusions

In this study, we analyzed the flow of a bio-convective hybrid nanofluid with non-Newtonian behavior (specifically, the Eyring–Powell fluid model) over a vertical cone and plate. This study also considered the effects of magnetohydrodynamics (MHD), thermal radiation, and chemical reactions to gain insights into the heat and mass transfer processes involved. The governing equations were solved using the Keller-box finite-difference scheme, transforming them into ordinary differential equations. We examined various physical aspect application numbers to comprehensively understand the model, and the results were compared to previous research findings, showing good agreement. The observations from this study revealed the following key findings:

1. When increasing the MHD (M) and Eyring–Powell fluid (K) parameters:
    - The heat transfer increased by 24.3% and 6.2%.

- The mass transfer increased by 17.4% and 4.5%.
- The microorganism diffusion increased by 18.2% and 4.1%.

2. When increasing the volume fraction (ϕ_1 and ϕ_2):
    - The heat transfer increased by 5.8%.
    - The mass transfer increased by 4.6%.
3. When increasing the thermal radiation (R_d) parameter:
    - Heat transfer increased by 16.4%.
    - The microorganism diffusion increased by 4.6%.
4. When decreasing the chemical reaction (K_r) parameter:
    - The mass transfer increased by 18.4%.

Author Contributions: Conceptualization, F.P. and P.S.; methodology, F.P.; software, F.P.; validation, F.P., P.S., and S.D.; formal analysis, F.P.; investigation, F.P.; resources, P.S.; data curation, P.S.; writing—original draft preparation, F.P.; writing—review and editing, P.S.; visualization, P.S.; supervision, P.S.; project administration, S.D.; funding acquisition, S.D. All authors have read and agreed to the published version of the manuscript.

Funding: This research received no external funding.

Data Availability Statement: All data are available within the manuscript.

Conflicts of Interest: The authors declare no conflict of interest.

Abbreviations

Nomenclature		**Greek Symbols**	
b	Chemotaxis constant	α_{hnf}	Thermal diffusivity of hybrid nanofluid
B_0^2	Magnetic parameter	β	Characteristics parameter of the Eyring–Powell fluid
C	Concentration	β_T, β_C	Volumetric expansion of thermal, concentration
Cp_{hnf}, Cp_f	Specific heat	γ	The average volume of microorganisms
d	Physical Eyring–Powell fluid parameter	θ	Dimensionless function of temperature
D	Mass diffusivity	μ_{hnf}, μ_f, μ_s	Dynamic viscosity
D_n	Diffusivity of microorganisms	ν_{hnf}, ν_f	Kinematic viscosity
K	Dimensionless Eyring–Powell parameter	ξ	Dimensionless boundary layer coordinate
K_r	Dimensionless chemical reaction parameter	ψ	Stream function
k_c	Dimensional chemical reaction parameter	$\rho_{hnf}, \rho_f, \rho_s$	Density
L_b	Bio-convection Lewis number	σ	Bio-convection constant
M	Dimensionless magnetic parameter	ϕ_1, ϕ_2	Volume fraction of nanofluid
N	Density of microorganisms	φ	Dimensionless function of concentration
N_1	Non-Newtonian fluid parameter	χ	Dimensionless function of microorganism density
N_r	Buoyancy ratio parameter		
P_r	Prandtl number	**Subscripts**	
P_e	Bio-convection Peclet number		
q_r	Dimensional thermal radiation	f	Condition of base fluid
R_b	Bio-convection Rayleigh number	hnf	Condition of hybrid nanofluid
R_d	Dimensionless thermal radiation parameter	nf	Condition of nanofluid
S_c	Schmidt number	s	Condition of nanoparticle
T	Temperature	w	Condition of wall
u, v	Velocity component	∞	Condition of ambient
W_c	The maximum cell swimming speed		
x, y	Coordinate		

References

1. Barth, W.L.; Carey, G.F. On a natural-convection benchmark problem in non-Newtonian fluids. *Numer. Heat Transf. Part B Fundam.* **2006**, *50*, 193–216. [CrossRef]
2. Patel, M.; Timol, M. Numerical treatment of Powell–Eyring fluid flow using method of satisfaction of asymptotic boundary conditions (MSABC). *Appl. Numer. Math.* **2009**, *59*, 2584–2592. [CrossRef]
3. Hanafi, H.; Shafie, S.; Ullah, I. Unsteady Free Convection Flow of Nanofluid with Dissipation Effect over a Non-Isothermal Vertical Cone. *J. Adv. Res. Fluid Mech. Therm. Sci.* **2020**, *75*, 1–11. [CrossRef]
4. Ragulkumar, E.; Sambath, P.; Chamkha, A.J. Free convection nanofluid flow past a vertical isothermal cone surface in the presence of viscous dissipation and MHD with heat flux. *Eur. Phys. J. Plus* **2022**, *137*, 894. [CrossRef]
5. Hering, R.; Grosh, R. Laminar free convection from a non-isothermal cone. *Int. J. Heat Mass Transf.* **1962**, *5*, 1059–1068. [CrossRef]
6. Lin, F. Laminar free convection from a vertical cone with uniform surface heat flux. *Lett. Heat Mass Transf.* **1976**, *3*, 49–58. [CrossRef]
7. Pop, I.; Watanabe, T. Free convection with uniform suction or injection from a vertical cone for constant wall heat flux. *Int. Commun. Heat Mass Transf.* **1992**, *19*, 275–283. [CrossRef]
8. Tripathi, R.; Sau, A.; Nath, G. Laminar free convection flow over a cone embedded in a stratified medium. *Mech. Res. Commun.* **1994**, *21*, 289–296. [CrossRef]
9. Hossain, M.; Paul, S. Free convection from a vertical permeable circular cone with non-uniform surface temperature. *Acta Mech.* **2001**, *151*, 103–114. [CrossRef]
10. Pullepu, B.; Ekambavanan, E.; Chamkha, A. Unsteady laminar natural convection from a non-isothermal vertical cone. *Nonlinear Anal. Model. Control* **2007**, *12*, 525–540. [CrossRef]
11. Sambath, P.; Kannan, R.; Pullepu, B. Free Convection Flow Past from Horizontally Inclined Plate in Thermally Stratified Medium. *Int. J. Pure Appl. Math.* **2017**, *114*, 313–322.
12. Pullepu, B.; Ekambavanan, K.; Chamkha, A. Unsteady laminar free convection from a vertical cone with uniform surface heat flux. *Nonlinear Anal. Model. Control* **2008**, *13*, 47–60. [CrossRef]
13. Hasan, M.; Mujumdar, A. Coupled heat and mass transfer in natural convection under flux condition along a vertical cone. *Int. Commun. Heat Mass Transf.* **1984**, *11*, 157–172. [CrossRef]
14. Sambath, P.; Sankar, D.; Viswanathan, K. A numerical study of dissipative chemically reactive radiative MHD flow past a vertical cone with nonuniform mass flux. *Int. J. Appl. Mech. Eng.* **2020**, *25*, 159–176. [CrossRef]
15. Atashafrooz, M.; Sajjadi, H.; Amiri Delouei, A. Simulation of combined convective-radiative heat transfer of hybrid nanofluid flow inside an open trapezoidal enclosure considering the magnetic force impacts. *J. Magn. Magn. Mater.* **2023**, *567*, 170354. [CrossRef]
16. Ragulkumar, E.; Palani, G.; Sambath, P.; Chamkha, A.J. Dissipative MHD free convective nanofluid flow past a vertical cone under radiative chemical reaction with mass flux. *Sci. Rep.* **2023**, *13*, 2878. [CrossRef] [PubMed]
17. Prabhavathi, B.; Sudarsanareddy, P.; Bhuvanavijaya, R. Three-Dimensional Heat and Mass Transfer Flow over a Stretching Sheet Filled with Al_2O_3-Water Based Nanofluid with Heat Generation/Absorption. *J. Nanofluids* **2019**, *8*, 1355–1361. [CrossRef]
18. Raju, C.; Jayachandrababu, M.; Sandeep, N.; Mohankrishna, P. Influence of non-uniform heat source/sink on MHD nanofluid flow over a moving vertical plate in porous medium. *Int. J. Sci. Eng. Res* **2015**, *6*, 31–42.
19. Kairi, R.; Murthy, P. Effect of viscous dissipation on natural convection heat and mass transfer from vertical cone in a non-Newtonian fluid saturated non-Darcy porous medium. *Appl. Math. Comput.* **2011**, *217*, 8100–8114. [CrossRef]
20. Jayachandra Babu, M.; Sandeep, N.; Raju, C.S. Heat and mass transfer in MHD Eyring-Powell nanofluid flow due to cone in porous medium. *Int. J. Eng. Res. Afr.* **2015**, *19*, 57–74. [CrossRef]
21. Rauf, A.; Abbas, Z.; Shehzad, S.; Alsaedi, A.; Hayat, T. Numerical simulation of chemically reactive Powell-Eyring liquid flow with double diffusive Cattaneo-Christov heat and mass flux theories. *Appl. Math. Mech.* **2018**, *39*, 467–476. [CrossRef]
22. Khan, M.; Irfan, M.; Khan, W.; Ahmad, L. Modeling and simulation for 3D magneto Eyring–Powell nanomaterial subject to nonlinear thermal radiation and convective heating. *Results Phys.* **2017**, *7*, 1899–1906. [CrossRef]
23. Kumar, B.; Srinivas, S. Unsteady hydromagnetic flow of Eyring-Powell nanofluid over an inclined permeable stretching sheet with joule heating and thermal radiation. *J. Appl. Comput. Mech.* **2020**, *6*, 259–270. [CrossRef]
24. Reddy, S.; Reddy, P.B.A.; Bhattacharyya, K. Effect of nonlinear thermal radiation on 3D magneto slip flow of Eyring-Powell nanofluid flow over a slendering sheet with binary chemical reaction and Arrhenius activation energy. *Adv. Powder Technol.* **2019**, *30*, 3203–3213. [CrossRef]
25. Manvi, B.; Tawade, J.; Biradar, M.; Noeiaghdam, S.; Fernandez-Gamiz, U.; Govindan, V. The effects of MHD radiating and non-uniform heat source/sink with heating on the momentum and heat transfer of Eyring-Powell fluid over a stretching. *Results Eng.* **2022**, *14*, 100435. [CrossRef]
26. Khan, Z.; Usman, M.; Zubair, T.; Hamid, M.; Haq, R. Brownian motion and thermophoresis effects on unsteady stagnation point flow of Eyring–Powell nanofluid: A Galerkin approach. *Commun. Theor. Phys.* **2020**, *72*, 125005. [CrossRef]
27. Thumma, T.; PV, S.N. Innovations in Eyring–Powell radiative nanofluid flow due to nonlinear stretching sheet with convective heat and mass conditions: Numerical study. *Aust. J. Mech. Eng.* **2020**, *21*, 221–233. [CrossRef]
28. Imran, M.; Abbas, Z.; Naveed, M. Flow of Eyring-Powell liquid due to oscillatory stretchable curved sheet with modified Fourier and Fick's model. *Appl. Math. Mech.* **2021**, *42*, 1461–1478. [CrossRef]

29. Lawal, M.O.; Kasali, K.B.; Ogunseye, H.A.; Oni, M.O.; Tijani, Y.O.; Lawal, Y.T. On the mathematical model of Eyring–Powell nanofluid flow with non-linear radiation, variable thermal conductivity and viscosity. *Partial Differ. Equ. Appl. Math.* **2022**, *5*, 100318. [CrossRef]
30. Tian, Q.; Yang, X.; Zhang, H.; Xu, D. An implicit robust numerical scheme with graded meshes for the modified Burgers model with nonlocal dynamic properties. *Comput. Appl. Math.* **2023**, *42*, 246. [CrossRef]
31. Chen, H.; Stynes, M. Blow-up of error estimates in time-fractional initial-boundary value problems. *IMA J. Numer. Anal.* **2021**, *41*, 974–997. [CrossRef]
32. Jiang, X.; Wang, J.; Wang, W.; Zhang, H. A Predictor–Corrector Compact Difference Scheme for a Nonlinear Fractional Differential Equation. *Fractal Fract.* **2023**, *7*, 521. [CrossRef]
33. Yang, X.; Wu, L.; Zhang, H. A space-time spectral order sinc-collocation method for the fourth-order nonlocal heat model arising in viscoelasticity. *Appl. Math. Comput.* **2023**, *457*, 128192. [CrossRef]
34. Pal, D.; Mondal, S.K. Unsteady magneto-bioconvection flow of chemically reactive powell eyring nanofluid having gyrotactic microorganisms over an inclined stretching sheet with non-uniform heat source/sink and thermal radiation. *J. Nanofluids* **2019**, *8*, 703–713. [CrossRef]
35. Alwatban, A.M.; Khan, S.U.; Waqas, H.; Tlili, I. Interaction of Wu's slip features in bioconvection of Eyring Powell nanoparticles with activation energy. *Processes* **2019**, *7*, 859. [CrossRef]
36. Sreenivasulu, P.; Poornima, T.; Malleswari, B.; Reddy, N.B.; Souayeh, B. Internal energy activation stimulus on magneto-bioconvective Powell-Eyring nanofluid containing gyrotactic microorganisms under active/passive nanoparticles flux. *Phys. Scr.* **2021**, *96*, 055221. [CrossRef]
37. Mahdy, A. Unsteady Mixed Bioconvection Flow of Eyring–Powell Nanofluid with Motile Gyrotactic Microorganisms Past Stretching Surface. *BioNanoScience* **2021**, *11*, 295–305. [CrossRef]
38. Naz, R.; Mabood, F.; Sohail, M.; Tlili, I. Thermal and species transportation of Eyring-Powell material over a rotating disk with swimming microorganisms: Applications to metallurgy. *J. Mater. Res. Technol.* **2020**, *9*, 5577–5590. [CrossRef]